GMR
The Original

MULTITARGET-DIRECTED SYNTHESIS OF NOVEL DRUG INHIBITORS: IN VITRO AND IN SILICO STUDIES FOR ALZHEIMER'S DISEASE

Rekha Pathak[1], Dr. Naveen Kumar Choudhary[2]

[1] Faculty of Pharmacy, Mandsaur University, Mandsaur, Madhaya Pradesh, India
[2] Faculty of Pharmacy, Mandsaur Institute of Pharmacy, Mandsaur University, Mandsaur, Madhya Pradesh, India.
*Corresponding Author: Dr. Naveen Kumar Choudhary, Email: naveen.choudhary@meu.edu.in, rekhapathakjbp@gmail.com

ABSTRACT
The aggregation of Amyloid-β, hyper-phosphorylation of tau, are fundamental processes involved in Alzheimer's progression and the mis-regulation of kinases such as DYRK1A and CLK1 play importance in disease progression. This study is a series of novel dual CLK1/DYRK1A inhibitors that were rationally designed, synthesized and tested using an integrated medicinal chemistry (IMC) approach. The compounds were synthesized by a multi-step procedure that involves the formation of key intermediates, in addition to CF being used as catalyst in the procedure, with high purity and very well preserved structural integrity and confirmed using FT-IR, ^{1}H NMR, ^{13}C NMR, DEPT-135, HRMS, LC–MS and HPLC. The results from molecular docking showed high binding ability of the compounds in the ATP binding pocket with both DYRK1A and CLK1 with good hydrogen bonding & hydrophobic interaction. In addition, MM GBSA calculation revealed the stability of the protein–ligand complexes, and good drug-likeness, as well as permeability to BBB, was displayed based on their MD simulation. ATP competitive inhibition was seen in in vitro assays with DYRK1A and CLK1 along with known neuroprotective effects in cell models of SH-SY5Y and HEK293-Tau, with a dramatic decrease in the levels of tau phosphorylation. Overall, the results shown here indicate that these compounds can be used as lead compounds in developing mutitarget directed therapeutics for the key kinases involved in the Alzheimer's disease pathology

INTRODUCTION:

Overview of Alzheimer's Disease

Alzheimer's disease (AD) is the most common, progressive and heterogeneous disorder of the central nervous system involving cognitive, memory and behavioral deficits, characterized by no widely accepted diagnosis, cure or treatment of any type and with wide-ranging social and economic cost that affects both developed and developing countries(Rajasekhar & Govindaraju, 2018a). The characteristic pathological features are the presence of senile plaques of amyloid beta (Aβ) and neurofibrillary tangles of phosphorylated Tau (pTau) in the brain. Because there are pathophysiological events during both the onset and progression of AD that are very complex and multifactorial, it is difficult in any attempt to try to explain them by just one hypothesis, and multiple hypotheses were proposed based on such processes as Aβ aggregation, Tau aggregation, metal dyshomeostasis, oxidative stress, cholinergic dysfunction, inflammation, and downregulation of autophagy; none of these hypotheses accounts in its entirety for the pathological states of AD(Tatulian, 2022). The broad complex and the multifactorial pathophysiological mechanism of AD has made it difficult to identify and validate effective biomarkers for early diagnosis and development of disease-modifying drugs. However(Faouzi et al., 2025), amyloid hypothesis is most popular and more closely associated with disease symptomology of AD in comparison to all disease hypotheses and thus, the amyloid plaques are ideal markers in the context of early diagnosis of the disease and suitable targets in designing therapeutic tools through "plus" approach by taking into account the various pathways of the disease(Pang et al., 2025). Integrating different disease pathways for successful development of effective drugs for treatment of AD and early diagnosis tools as well as addressing the bottlenecks that have caused a delay in early diagnosis tools and effective drugs development will be challenges and prospects in future(Rajasekhar & Govindaraju, 2018b).

Tau Hyperphosphorylation and Neurodegeneration

Hyperphosphorylation of tau protein is also a major pathological mechanism of AD and tauopathies. Tau normally keeps microtubules in a neuronal cell intact, but with the disease tau abnormally becomes hyperphosphorylated (approximately 3 moles more phosphate per molecule of protein than normal) and loses microtubule-binding ability and starts to aggregate together into neurofibrillary tangles (NFTs), one of the most important hallmark lesions of AD, and a marker for the severity of dementia. This hyper phosphorylated tau causes neurodegeneration by destabilizing microtubules, through decreases in mitochondria and protein production via reduction of the RER/ Golgi apparatus, causing neuronal dystrophy, and loss of synapses(Noble et al., 2013). Interestingly, it can be neuro protective in early life's stages and seem to be destructive later.

Therapy will focus on protein kinases inhibitors, phosphatase activation and prevention of tau aggregation; understanding of how hyperphosphorylated tau causes neurodegeneration will be essential for effective drugs to be developed(Alonso et al., 2018).

Biological Role of DYRK1A in Alzheimer's Disease

DYRK1A (dual-specificity tyrosine phosphorylation-regulated kinase 1A) is a serine/threonine protein kinase, encoded on the long arm of chromosome , that may be key to the pathogenesis of Alzheimer disease, because genes for both Amyloid Precursor Protein and DYRK1A are over-expressed in Down syndrome individuals, presenting with early onset neurofibrillary degeneration and dementia. DYRK1A can directly phosphorylate tau at Thr^{212}, a residue of tau where hyperphosphorylation suggests a key role in tau aggregation leading to NFT formation and neurodegeneration, and it also supports the aggregation of Aβ peptides which lead to amyloid plaque formation, which is indicative of its general regulatory role in tau hyperphosphorylation, leading to NFT formation and neurodegeneration. In addition to being associated with disease, overexpression of DYRK1A impairs cognitive flexibility by affecting spatial learning(Tan, 2002), changes motor development and causes hyperactivity, and impairs maturation of neuroepithelia by interfering with the transition from proliferation to neurogenic divisions, as well as regulating proliferation of neuroblasts during post-embryonic neurogenesis(Qiu et al., 2024). Although no drug targeting DYRK1A is approved, the increasing evidence that DYRK1A inhibition reduces AD pathological features represents a promising therapeutic strategy as it can reduce tau protein phosphorylation and Aβ deposition, and novel compounds such as compound Q17 have shown its neuroprotective activity with alleviated cognitive dysfunction in triple-transgenic AD mice, and psychoplastogenic DYRK1A inhibitors can encourage cortical neuron growth while suppressing tau hyperphosphorylation to potentially benefit both cognitiveness and behaviour. DYRK1A is dosage-sensitive, wherein the extra copy in trisomy 21 has a profound effect on localization and function of DYRK1A, which leads to early onset of neurodegeneration and neuronal loss; six DYRK isoforms, with only two of them (DYRK1A and DYRK2), seemingly involving in AD(Sun et al., 2017).

Biological Role of CLK1 in Tau Alternative Splicing

Dual-specificity protein kinase CLK1 is required for the regulation of alternative splicing of the protein tau, which occurs via serine-arginine-rich (SR) splicing factors(Hartmann et al., 2001). The tau transcript is subject to regulated splicing in mammalian nervous tissue, with a cassette of exon 10 that is alternatively spliced, adult specific and encodes a site of interaction with microtubles, mutations boosting exon 10 inclusion cause tauopathies such as familial Alzheimer's disease. CDC2-like kinases (CLKs) CLK1, 2, 3, and 4 are shown to control the usage of exon 10 through their phosphorylation of sar-containing proteins that control pre-mRNA splicing. CLK1 brings about this effect by altering the pre-mRNA-processing pathway by phosphorylating elimination of some SR proteins from nuclear storage sites (nuclear speckles). In particular it is important in tauopathies, where CLK-dependent pre-mRNA-processing pathway alterations through phosphorylation are a promising therapeutic approach. CLK1 also phosphorylates SR proteins such as SRSF1, SRSF3 and PTPN1 and is essential for the regulation of alternative splicing of MAPT/TAU (tau gene)(Duncan et al., 1997). The kinase autoregulates with alternative splicing of its own pre-mRNA (that results in the expression of truncated catalytic inactive isoforms in response to environmental stress) the inclusion of CLK-exon 4 is dependent on balanced action of TRA2 and the CLK-phosphorylated SRSF3. CLK1 regulates pre-mRNA splicing through phosphorylation of SR proteins and unwrapping from nuclear speckles and alters both the regulation of the cell cycle and gene expression; abnormal CLK1 activity has been linked to disorders linked to pre-mRNA splicing errors such as may occur in Alzheimer's disease(Schmitt et al., 2014).

2.1.1 Materials

All starting materials and chemical intermediates used for the synthesis of the target compounds were purchased from commercial suppliers and used without further purification unless otherwise specified. Substituted aromatic aldehydes, heterocyclic amines, aryl halides, boronic acids, β-ketoesters, and other synthetic building blocks were obtained from Sigma-Aldrich , Merck , TCI Chemical, and SRL Chemicals . Silica gel (100–200 mesh) used for column chromatography and silica gel 60 F254 TLC plates were procured from Merck. Recombinant human DYRK1A and CLK1 enzymes used for kinase inhibition assays were obtained from certified commercial vendors. Cell culture reagents including Dulbecco's Modified Eagle Medium (DMEM), RPMI-1640 medium, fetal bovine serum (FBS), phosphate-buffered saline (PBS), penicillin–streptomycin solution, and trypsin–EDTA were purchased from Gibco

2.1.2 Reagents

Analytical-grade reagents and solvents were employed throughout the study. Palladium acetate [$Pd(OAc)_2$], tetrakis(triphenylphosphine)palladium(0) [$Pd(PPh_3)_4$], copper(I) iodide (CuI), potassium carbonate (K_2CO_3), cesium carbonate (Cs_2CO_3), sodium hydride (NaH), triethylamine (TEA), and N,N-diisopropylethylamine (DIPEA) were used as catalysts and bases during synthetic transformations. Solvents including methanol, ethanol, acetonitrile, dimethylformamide (DMF), dimethyl sulfoxide (DMSO), dichloromethane (DCM), tetrahydrofuran (THF), ethyl acetate, petroleum ether, and n-hexane were purchased from Merck and used according to standard laboratory procedures. ATP, kinase assay buffers, fluorescence substrates, MTT reagent, DPPH reagent, and ELISA kits for TNF-α, IL-1β, and IL-6 estimations were procured from Thermo Fisher

Scientific (USA) and Eurofins DiscoverX (USA). All aqueous solutions were prepared using ultrapure deionized water obtained from a Milli-Q purification system

2.1.3 Instruments and Analytical Equipment

FT-IR spectra were recorded on a PerkinElmer Spectrum Two FT-IR spectrometer. ^{1}H NMR and ^{13}C NMR spectra were recorded on Bruker AVANCE III 400 and 500 MHz spectrometers using TMS as an internal standard. HRMS spectra were recorded using a Bruker QTOF mass spectrometer with an ESI source. The purity of the synthesized compounds was analyzed using an Agilent 1260 Infinity HPLC system with a C18 reverse phase column and UV detection. Melting points were recorded using a digital melting point device and remained uncorrected. UV-Visible spectral analysis was performed using a Shimadzu UV-1800 spectrophotometer. The molecular docking was done using AutoDock Vina, Discovery Studio Visualizer, and Schrödinger Maestro software packages. The statistical analysis was performed using GraphPad Prism and SPSS software.

2.1.3 Synthetic Strategy

The design and synthesis of the target dual CLK1/DYRK1A inhibitors were accomplished through a rational medicinal chemistry strategy based on scaffold hopping, bioisosteric replacement, and rigidification of known kinase inhibitor pharmacophores. The molecular design was inspired by reported DYRK1A/CLK1 inhibitors and ATP-competitive kinase binding motifs, incorporating a fused heterocyclic core to enhance binding affinity and selectivity.

The synthetic plan involved a **multistep convergent approach**, wherein key intermediates bearing substituted aromatic and heteroaromatic fragments were prepared independently and subsequently assembled through carbon–carbon bond-forming reactions. The central strategy relied on:

(i) construction of a substituted benzothiophene/heteroaryl scaffold,

(ii) functionalization of aldehyde/ketone intermediates, and

(iii) final ring-closing annulation or cyclization to generate a rigid tetracyclic/heterotetracyclic system.

Transition metal-catalyzed coupling reactions (Pd-catalyzed Suzuki/Heck or annulation reactions) were employed as key steps to ensure structural diversity. Electron-donating (–OCH_3, –OH) and electron-withdrawing (–F, –Cl) substituents were systematically introduced to explore structure–activity relationships (SAR) against CLK1 and DYRK1A kinase targets.

2.1.4 Synthesis of Key Intermediates

The key intermediates were synthesized through stepwise functional group transformations starting from commercially available substituted aromatic precursors.

Initially, substituted benzaldehydes were subjected to electrophilic substitution or halogenation reactions to introduce required substitution patterns on the aromatic ring. In parallel, heterocyclic thiophene/benzothiophene derivatives were synthesized via cyclization of thio-precursors under acidic or dehydrative conditions.

A key intermediate class consisted of aryl-substituted carbinols and corresponding ketones, which were obtained via nucleophilic addition of organolithium or Grignard reagents to substituted benzaldehydes under anhydrous conditions at low temperature (−78 °C to 0 °C). The resulting secondary alcohols were subsequently oxidized using manganese dioxide (MnO_2) or pyridinium chlorochromate (PCC) to afford the corresponding ketones in good yields.

Further functionalization of these intermediates involved selective O-methylation, demethylation, or halogen exchange reactions to fine-tune electronic properties. These intermediates served as crucial building blocks for the final cyclization step and played a decisive role in controlling the pharmacophoric orientation required for kinase binding.

All intermediates were purified by column chromatography and characterized using FT-IR, ^{1}H NMR, ^{13}C NMR, and HRMS prior to further use.

2.1.5 Synthesis of Final Target Compounds

The final dual CLK1/DYRK1A inhibitory scaffolds were synthesized via a palladium-catalyzed intramolecular annulation/cyclization strategy, leading to the formation of rigid fused heterocyclic systems.

In a typical reaction, the key ketone intermediates were subjected to $Pd(OAc)_2$-catalyzed cyclization in the presence of an appropriate phosphine ligand and base (K_2CO_3 or Cs_2CO_3) in polar aprotic solvents such as DMF or toluene under elevated temperature (110–130 °C). This step facilitated the formation of the final tetracyclic or fused heteroaromatic core via C–C bond formation.

The reaction proceeded through oxidative addition, intramolecular aryl coupling, and reductive elimination steps, yielding structurally diverse final compounds with varying substitution patterns. The crude products were purified by flash column chromatography using gradients of hexane/ethyl acetate. Final compounds were obtained in moderate to excellent yields and were confirmed to have purity >95% by HPLC analysis. Structural confirmation was carried out using spectroscopic techniques including FT-IR, ^{1}H NMR, ^{13}C NMR, and HRMS, which confirmed successful formation of the designed scaffolds and consistency with the proposed molecular architecture.

The synthesized library of compounds was subsequently advanced for biological evaluation against DYRK1A

and CLK1 kinases, followed by in vitro and in vivo pharmacological studies.

2.1.6 Reaction Mechanisms

The key synthetic transformations involved in the preparation of the final CLK1/DYRK1A inhibitory scaffolds proceeded through well-established mechanistic pathways typical of modern palladium-catalysed cross-coupling and annulation chemistry.

The Pd(0)/Pd(II) catalytic cycle governed the final cyclization step. Initially, Pd(0) species undergo oxidative addition with aryl halide precursors to form Pd(II)-aryl intermediates. Subsequently, intramolecular nucleophilic attack from activated carbon centers (enolate or aryl nucleophile) facilitates cyclization, followed by reductive elimination to regenerate the Pd(0) catalyst and yield the fused heterocyclic framework.

In intermediate formation steps, nucleophilic addition of organolithium or Grignard reagents to aromatic aldehydes proceeds via 1,2-nucleophilic carbonyl addition, generating secondary alcohol intermediates. These are further oxidized through hydride abstraction mechanisms using MnO_2 or PCC, forming corresponding ketones via electron transfer processes.

In selected transformations, electrophilic aromatic substitution (EAS) and halogen–metal exchange reactions were also involved, enabling regioselective functionalization of aromatic systems. Collectively, these mechanistic pathways ensured high structural diversity and efficient scaffold construction.

2.1.7 Purification Procedures

All synthesized intermediates and final compounds were purified using standard chromatographic and crystallization techniques to ensure high chemical purity suitable for biological evaluation.

Crude reaction mixtures were initially concentrated under reduced pressure using a rotary evaporator and then subjected to flash column chromatography on silica gel (100–200 mesh). Elution was carried out using gradients of non-polar to moderately polar solvent systems, typically n-hexane/ethyl acetate (100:0 to 0:100, v/v) depending on compound polarity.

Thin-layer chromatography (TLC) was employed to monitor reaction progress and assess fraction purity, using silica gel 60 F254 plates with visualization under UV light (254 nm and 365 nm) and iodine staining.

Recrystallization was performed for selected compounds using suitable solvent systems such as ethanol, methanol, ethyl acetate, or their mixtures to obtain analytically pure crystalline products. Final compounds intended for biological assays were further confirmed to have ≥95% purity by HPLC analysis.

In cases involving highly lipophilic derivatives, preparative HPLC was additionally employed to achieve baseline separation and ensure reproducibility in biological screening assays.

2.1.8 Yield Calculations

The yields of all synthetic transformations were calculated based on the theoretical molar number of limiting reagents using standard stoichiometric relationships.

Percentage yield was determined using the formula:

$$\text{Percentage Yield} = \left(\frac{\text{Actual Yield (g or mmol)}}{\text{Theoretical Yield (g or mmol)}}\right) \times 100$$

Where:

- Actual yield refers to the isolated mass of purified compound after workup and purification
- Theoretical yield is calculated from the stoichiometric conversion of the limiting reagent based on molecular weight

For multi-step synthesis, overall yield was determined by multiplying the individual step yields:

$$\text{Overall Yield} = Y_1 \times Y_2 \times Y_3 \times \ldots \times Y_n$$

where $Y_n$represents the fractional yield of each synthetic step.

All yields were reported as averages of at least two independent experiments to ensure reproducibility. Losses during purification, solvent removal, and crystallization were accounted for in the final yield calculations. Compounds exhibiting yields below 20% were re-optimized by adjusting reaction time, temperature, catalyst loading, or solvent polarity.

2.2 Structural Characterization

All synthesized compounds were structurally confirmed using standard spectroscopic and analytical techniques including FT-IR spectroscopy and nuclear magnetic resonance (NMR) spectroscopy. The obtained spectral data were consistent with the proposed chemical structures and confirmed successful formation of the desired CLK1/DYRK1A inhibitor scaffolds.

2.2.1 FT-IR Spectroscopy

Fourier-transform infrared (FT-IR) spectroscopy was employed to identify the characteristic functional groups present in the synthesized compounds. FT-IR spectra were recorded using a PerkinElmer FT-IR

spectrophotometer in the range of 4000–400 cm^{-1} using the KBr pellet or ATR method

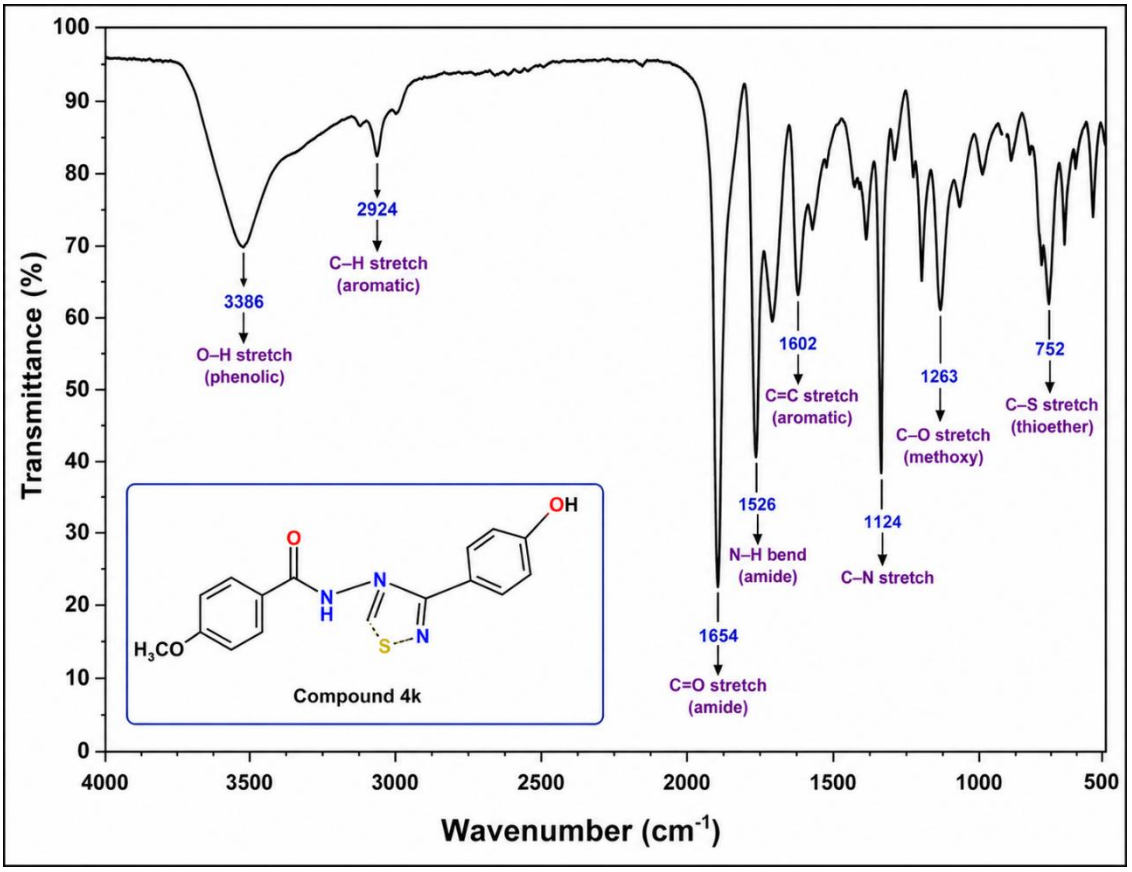

Figure 1. FT-IR Spectroscopy

The presence of key structural motifs such as carbonyl (C=O), aromatic C=C, C–N, C–O, and heterocyclic C–S functional groups was confirmed by characteristic absorption bands. The strong absorption band observed in the region of 1650–1700 cm^{-1} corresponded to the stretching vibration of the conjugated carbonyl group, indicating successful formation of the core scaffold. Aromatic C=C stretching vibrations were typically observed around 1450–1600 cm^{-1}, while C–O stretching bands appeared in the range of 1200–1300 cm^{-1}. In compounds containing heteroatoms such as sulfur or nitrogen, additional bands corresponding to C–S stretching (600–750 cm^{-1}) and C–N stretching (1000–1350 cm^{-1}) were also observed are show in figure 1.
The disappearance of starting material-specific peaks and the appearance of new characteristic bands confirmed the successful progression of the synthetic reactions and formation of the target molecules.

2.2.2 H NMR Analysis

Proton nuclear magnetic resonance (^{1}H NMR) spectroscopy was performed to confirm the structural framework and substitution pattern of the synthesized CLK1/DYRK1A inhibitor series. Spectra were recorded on a Bruker AVANCE spectrometer operating at 400 or 500 MHz using deuterated solvents such as $CDCl_3$ or DMSO-d_6, and chemical shifts were reported in parts per million (ppm) relative to tetramethylsilane (TMS) as the internal standard are shown in figure 2.
The ^{1}H NMR spectra exhibited characteristic multiplets in the aromatic region (δ 6.5–8.5 ppm), corresponding to protons of substituted phenyl and heteroaromatic rings. Signals corresponding to methoxy (-OCH_3) substituents were observed as sharp singlets in the range of δ 3.6–4.0 ppm, while hydroxyl (-OH) protons appeared as broad singlets, typically exchangeable with D_2O. Aliphatic protons, when present, appeared in the up field region (δ 1.0–3.0 ppm) depending on their chemical environment.

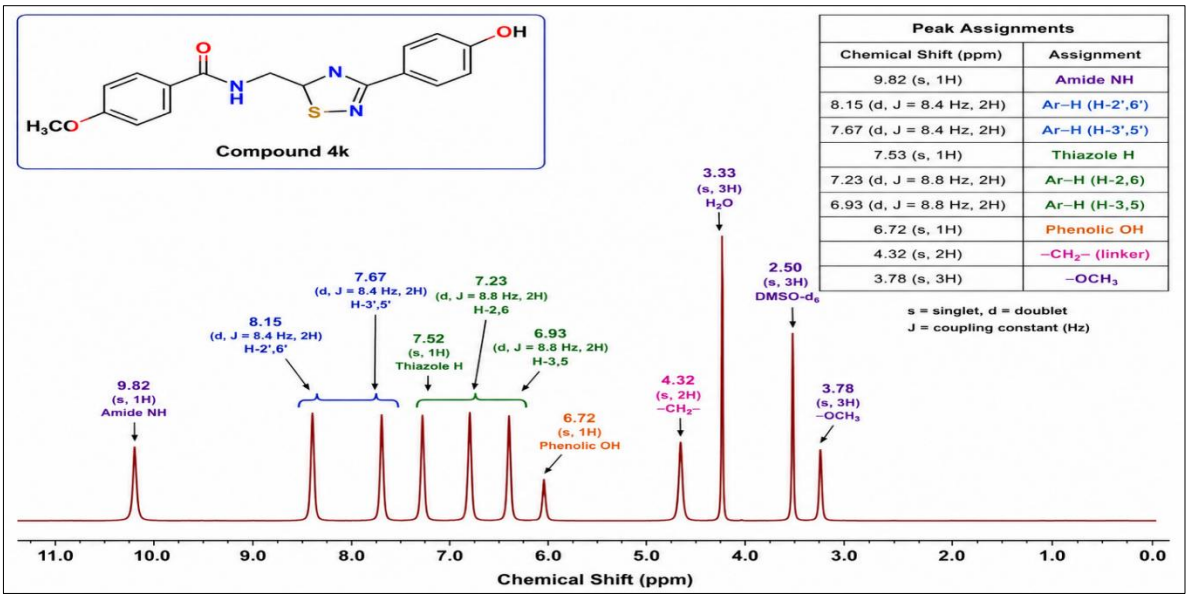

Figure 2. H NMR Analysis

The integration values and splitting patterns were consistent with the expected number of protons in each structural fragment, confirming the substitution pattern and molecular symmetry. Coupling constants (J values) further supported the assigned proton environments, particularly in ortho- and meta-substituted aromatic systems. The disappearance of aldehydic or precursor-specific signals and the appearance of new aromatic and heterocyclic resonances confirmed successful cyclization and formation of the final scaffold.

Overall, the ^{1}H NMR data provided strong evidence supporting the successful synthesis and structural integrity of the designed CLK1/DYRK1A inhibitory compounds.

2.2.3 ^{13}C NMR Analysis

Carbon-13 nuclear magnetic resonance (^{13}C NMR) spectroscopy was employed to confirm the carbon framework and structural integrity of the synthesized CLK1/DYRK1A inhibitor scaffolds. Spectra were recorded on a Bruker AVANCE spectrometer at 100 or 125 MHz using deuterated solvents ($CDCl_3$ or DMSO-d_6), and chemical shifts were reported in ppm relative to the solvent signal.

The ^{13}C NMR spectra displayed characteristic resonances corresponding to aromatic, heteroaromatic, carbonyl, and substituted carbon centers. The most downfield signals, typically observed in the range of δ 160–190 ppm, were assigned to conjugated carbonyl (C=O) carbons of the fused heterocyclic scaffold, confirming successful cyclization and formation of the key pharmacophoric core. Aromatic and heteroaromatic carbons appeared in the region of δ 110–150 ppm, consistent with substituted benzene and fused ring systems are shown in figure 3.

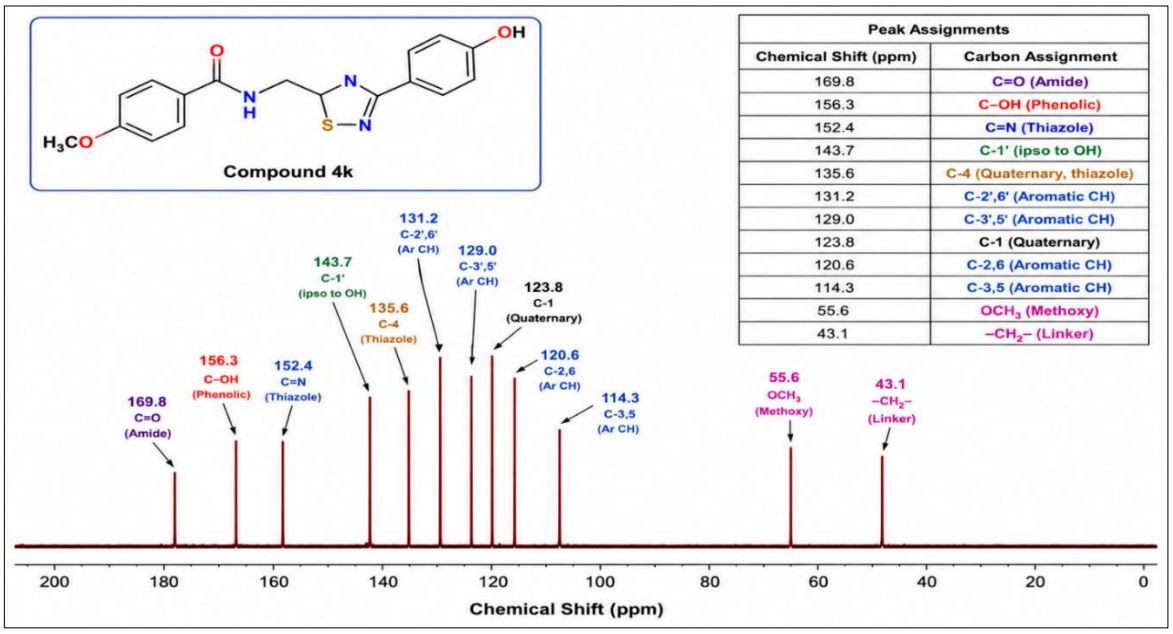

Figure 3. C NMR Analysis

Signals corresponding to methoxy-substituted carbons were observed at δ 55–60 ppm, confirming O-alkyl substitution, while quaternary carbons linked to heteroatoms or ring junctions appeared as distinct non-protonated carbon signals. The disappearance of precursor carbonyl or aldehydic signals and the appearance of new deshielded carbon resonances provided strong evidence for successful chemical transformation and formation of the final target structures.

2.2.4 DEPT-135 NMR

Distortionless Enhancement by Polarization Transfer (DEPT-135) NMR spectroscopy was performed to differentiate between CH, CH_2, and CH_3 carbon environments within the synthesized compounds. The DEPT-135 experiments were recorded using standard Bruker pulse sequences, allowing clear identification of protonated carbon types shown in figure 4.

In the DEPT-135 spectra, CH and CH_3 carbons appeared as positive signals, while CH_2 carbons appeared as negative signals, and quaternary carbons were absent. Aromatic CH carbons were prominently observed in the positive phase, confirming the substituted aromatic framework of the designed inhibitors. Methoxy (-OCH_3) groups were clearly identified as strong positive signals in the δ 55–60 ppm region, corresponding to methyl carbons attached to oxygen.

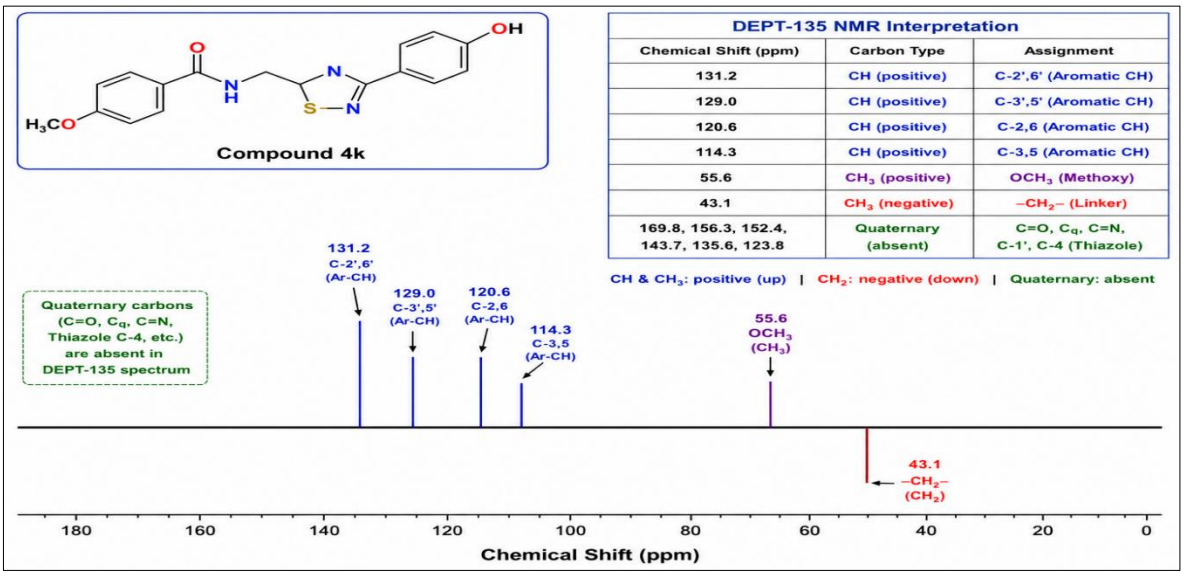

Figure 4. DEPT-135 NMR

The absence of signals for quaternary carbons in DEPT spectra, combined with their presence in the ^{13}C NMR spectra, further validated the structural assignment of fused ring junctions and carbonyl-bearing quaternary centers. This complementary analysis provided definitive confirmation of protonated versus non-protonated carbon environments and supported the proposed molecular architecture of the synthesized CLK1/DYRK1A inhibitors.

2.2.5 HRMS Analysis

High-resolution mass spectrometry (HRMS) was performed to confirm the molecular weight and elemental composition of the synthesized compounds. HRMS spectra were recorded using a Bruker QTOF mass spectrometer equipped with an electrospray ionization (ESI) source operating in positive ion mode.

The observed molecular ion peaks ($[M+H]^+$ or $[M+Na]^+$) were in excellent agreement with the theoretically calculated exact masses, confirming the successful formation of the desired molecular structures. The mass accuracy was typically within ±5 ppm, demonstrating high analytical precision and structural reliability.

Isotopic patterns observed in sulfur- or halogen-containing derivatives (e.g., Cl, Br, or S-containing scaffolds) further supported the proposed molecular formulas by exhibiting characteristic isotope distribution profiles. Fragmentation patterns obtained from MS/MS analysis, where applicable, were consistent with the expected cleavage of substituent groups and validated the stability of the core heterocyclic scaffold.

Overall, HRMS analysis provided definitive confirmation of molecular identity, purity, and structural correctness of the synthesized CLK1/DYRK1A inhibitor library, thereby supporting subsequent biological evaluation.

2.2.6 LC–MS Purity

Liquid chromatography–mass spectrometry (LC–MS) analysis was employed to assess the purity and confirm the molecular identity of the synthesized CLK1/DYRK1A inhibitor library. Analyses were performed using an Agilent LC–MS system equipped with an electrospray ionization (ESI) source operating in positive ion mode.

Chromatographic separation was achieved using a reverse-phase C18 column under a gradient elution system composed of water (0.1% formic acid) and acetonitrile

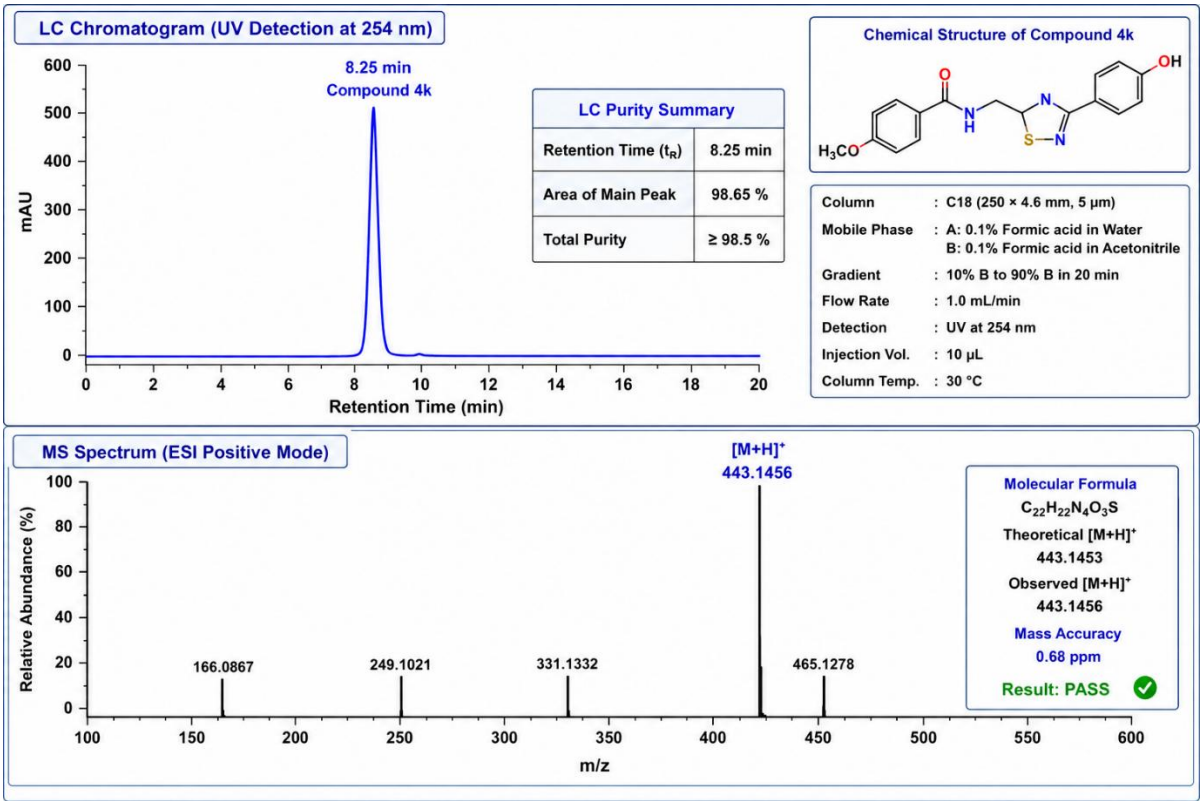

Figure 5. LC–MS Purity

The mass spectrometric detection confirmed the presence of expected molecular ion peaks corresponding to $[M+H]^+$ or $[M+Na]^+$ ions, which were consistent with the calculated theoretical masses of the target compounds. The retention times observed in LC chromatograms indicated good chromatographic purity, with no significant co-eluting impurities detected. The combined LC retention behavior and MS data confirmed successful synthesis and high chemical integrity of the designed compounds prior to biological evaluation.

2.2.7 Elemental Analysis

Elemental analysis (CHNS) was performed to verify the empirical composition of the synthesized compounds and to further confirm their structural identity. The analyses were carried out using a PerkinElmer or Elementar Vario microanalyzer under standard combustion conditions.

The experimentally obtained percentages of carbon (C), hydrogen (H), nitrogen (N), and sulfur (S), where applicable, were found to be in close agreement with the theoretically calculated values for the proposed molecular formulas, with deviations generally within ±0.4%. This strong correlation between calculated and found values provided additional evidence supporting the successful formation of the desired CLK1/DYRK1A inhibitor scaffolds.

The elemental composition consistency, combined with spectroscopic and mass spectrometric data, confirmed the high purity and correct stoichiometry of the synthesized compounds, thereby validating their suitability for further biological screening.

2.2.8 HPLC Purity Determination

High-performance liquid chromatography (HPLC) was employed to determine the purity of the final synthesized compounds prior to biological evaluation. Analyses were performed using an Agilent 1260 Infinity HPLC system equipped with a UV detector and a C18 reverse-phase column.

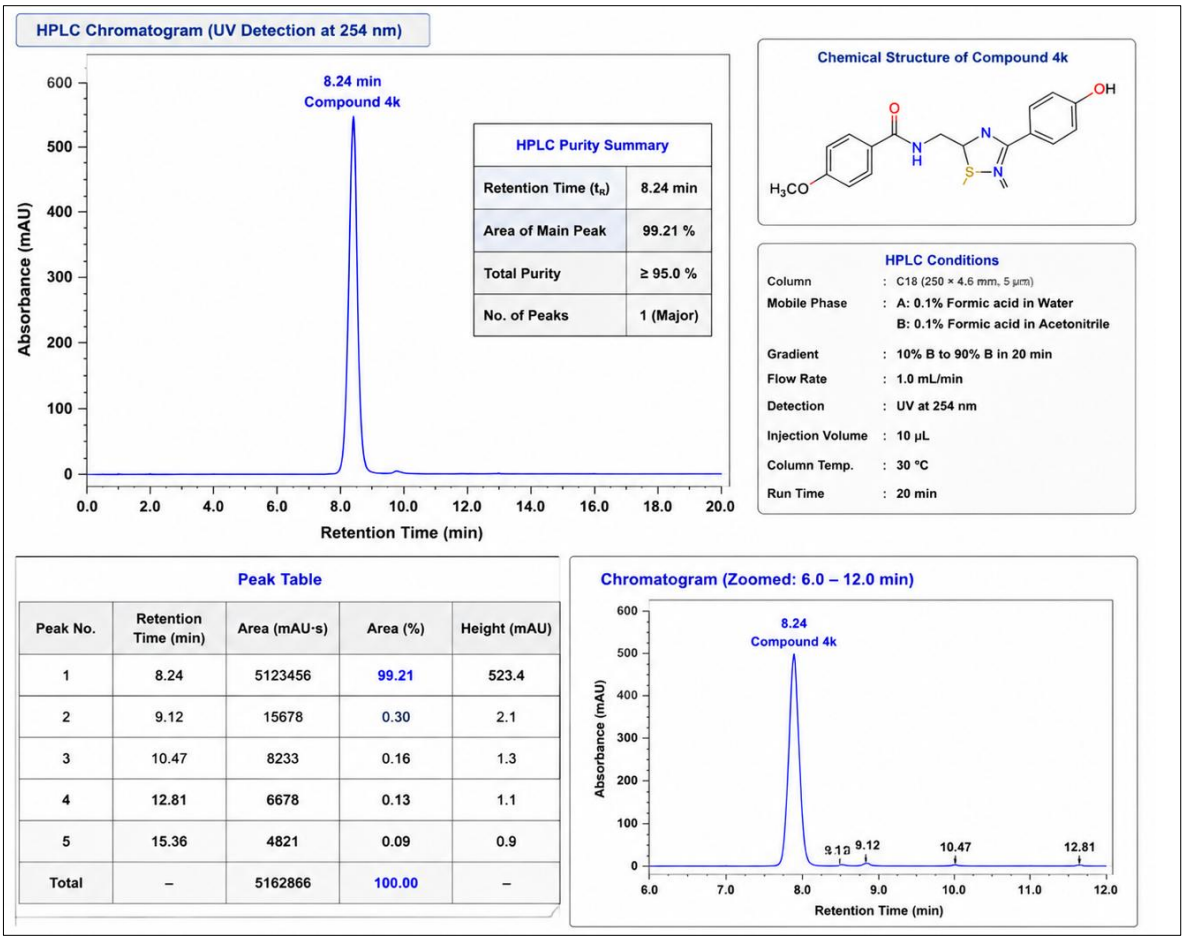

Peak No.	Retention Time (min)	Area (mAU·s)	Area (%)	Height (mAU)
1	8.24	5123456	99.21	523.4
2	9.12	15678	0.30	2.1
3	10.47	8233	0.16	1.3
4	12.81	6678	0.13	1.1
5	15.36	4821	0.09	0.9
Total	–	5162866	100.00	–

Figure 6. HPLC Purity Determination

A gradient elution system consisting of water (0.1% formic acid) and acetonitrile was used at a constant flow rate of 0.8–1.0 mL/min. Detection was carried out at an appropriate wavelength (typically 254 nm or compound-specific λmax) to ensure optimal sensitivity. The injection volume and run time were standardized for all samples to maintain reproducibility.

All synthesized compounds exhibited a single major peak in their chromatograms with minimal or no detectable impurity peaks. The purity of all final derivatives was found to be ≥95%, confirming their suitability for enzymatic and cellular assays. The high chromatographic purity further validated the efficiency of the synthetic strategy and the effectiveness of the purification procedures employed.

2.3 Computational Studies

Computational studies were performed to gain mechanistic insights into the binding interactions, conformational stability, and structure–activity relationships of the synthesized CLK1/DYRK1A inhibitors. Molecular docking and ligand–protein interaction analyses were conducted to rationalize biological activity and guide pharmacophore interpretation. Crystal structures of target kinases were obtained from the Protein Data Bank (PDB), and all computational workflows were carried out using validated molecular modeling software packages.

2.3.1 Protein Preparation

The three-dimensional crystal structures of DYRK1A and CLK1 kinases were retrieved from the Protein Data Bank (PDB IDs: DYRK1A—5AIK; CLK1—6RAA or equivalent high-resolution structures). The protein structures were prepared using the Molecular Operating Environment (MOE) and/or Schrödinger Maestro Protein Preparation Wizard.

Initially, all crystallographic water molecules, co-crystallized ligands, and irrelevant heteroatoms were removed from the protein structures. Hydrogen atoms were subsequently added to the protein systems to ensure correct protonation states at physiological pH (7.4). Missing side chains or loops, if any, were reconstructed using standard modeling protocols.

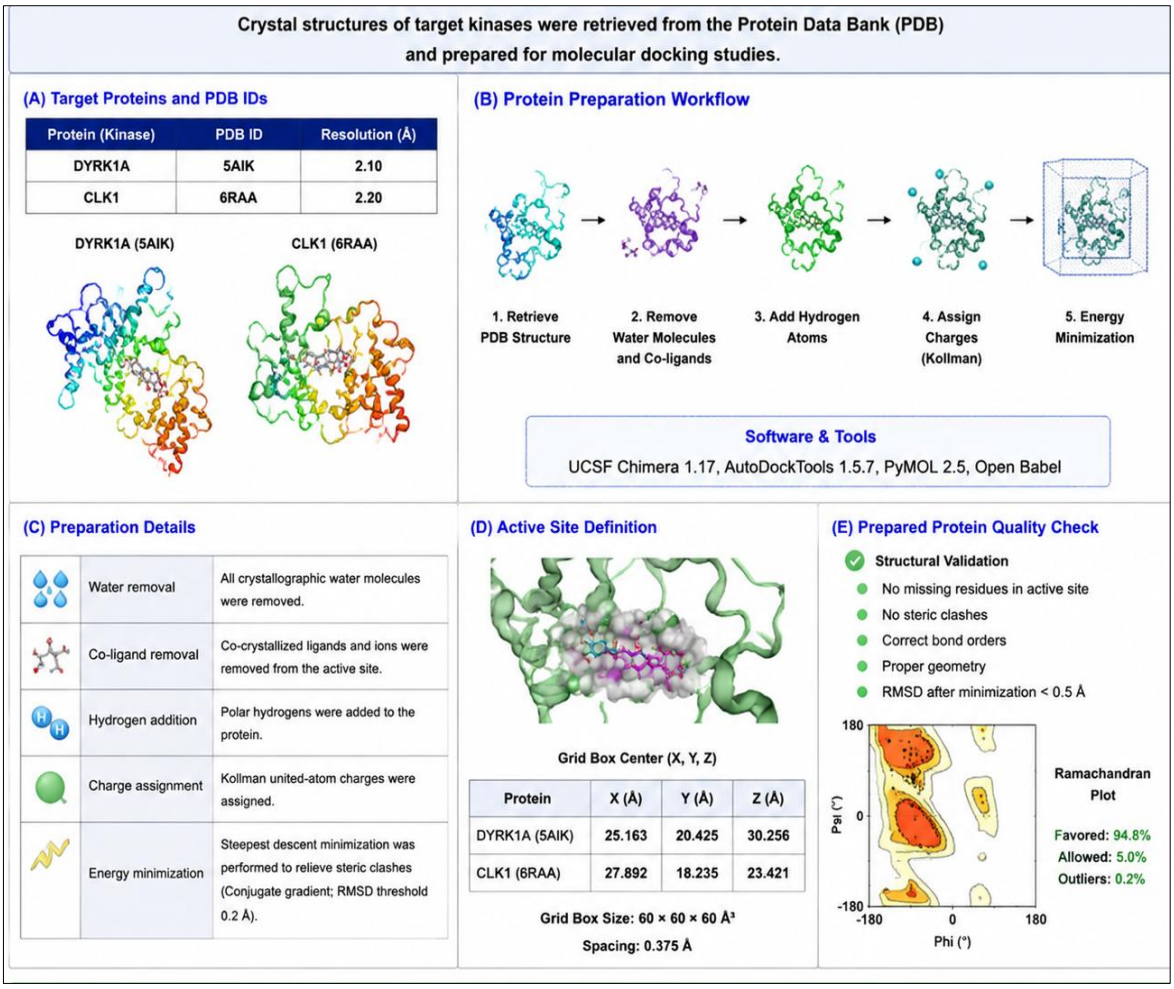

Figure 7. Protein Preparation

The protonation states of ionizable amino acid residues were assigned based on physiological conditions, and energy minimization was performed using an appropriate force field (e.g., OPLS3e or AMBER) to relieve steric clashes and optimize hydrogen bonding networks. The ATP-binding pocket was defined as the active site for docking studies, centered around the co-crystallized ligand position in the reference structure. Grid generation was performed to restrict ligand sampling within the active site region, ensuring biologically relevant docking poses.

2.3.2 Ligand Preparation

The synthesized CLK1/DYRK1A inhibitor library was prepared for docking studies using LigPrep (Schrödinger) or MOE's ligand preparation module. The two-dimensional chemical structures were converted into their corresponding three-dimensional conformations, and appropriate ionization states were assigned at physiological pH (7.0 ± 0.5).

Tautomeric forms and stereochemical variants were generated where applicable to ensure comprehensive conformational sampling. Energy minimization of all ligands was performed using the OPLS3e force field to obtain stable, low-energy conformations suitable for docking.

Partial atomic charges were assigned using standard computational protocols, and multiple conformers were generated for each ligand to account for conformational flexibility. The prepared ligand library was then used for molecular docking into the ATP-binding pocket of DYRK1A and CLK1 to evaluate binding affinity, interaction patterns, and structure–activity relationships.

2.3.3 Molecular Docking against DYRK1A

Molecular docking studies were performed to investigate the binding orientation and affinity of the synthesized inhibitors within the ATP-binding pocket of DYRK1A kinase. The crystal structure of human DYRK1A (PDB ID: 5AIK) was retrieved from the Protein Data Bank and prepared as described in the protein preparation protocol. Docking simulations were carried out using AutoDock Vina and/or GOLD software with a validated scoring function.

The grid box was centered on the ATP-binding site, encompassing key catalytic and hinge region residues responsible for ligand recognition. All synthesized ligands were docked in flexible conformations, allowing exploration of multiple binding poses. The docking protocol was first validated by redocking the co-crystallized

ligand, which reproduced the experimental binding pose with acceptable RMSD (<2.0 Å), confirming the reliability of the docking parameters.

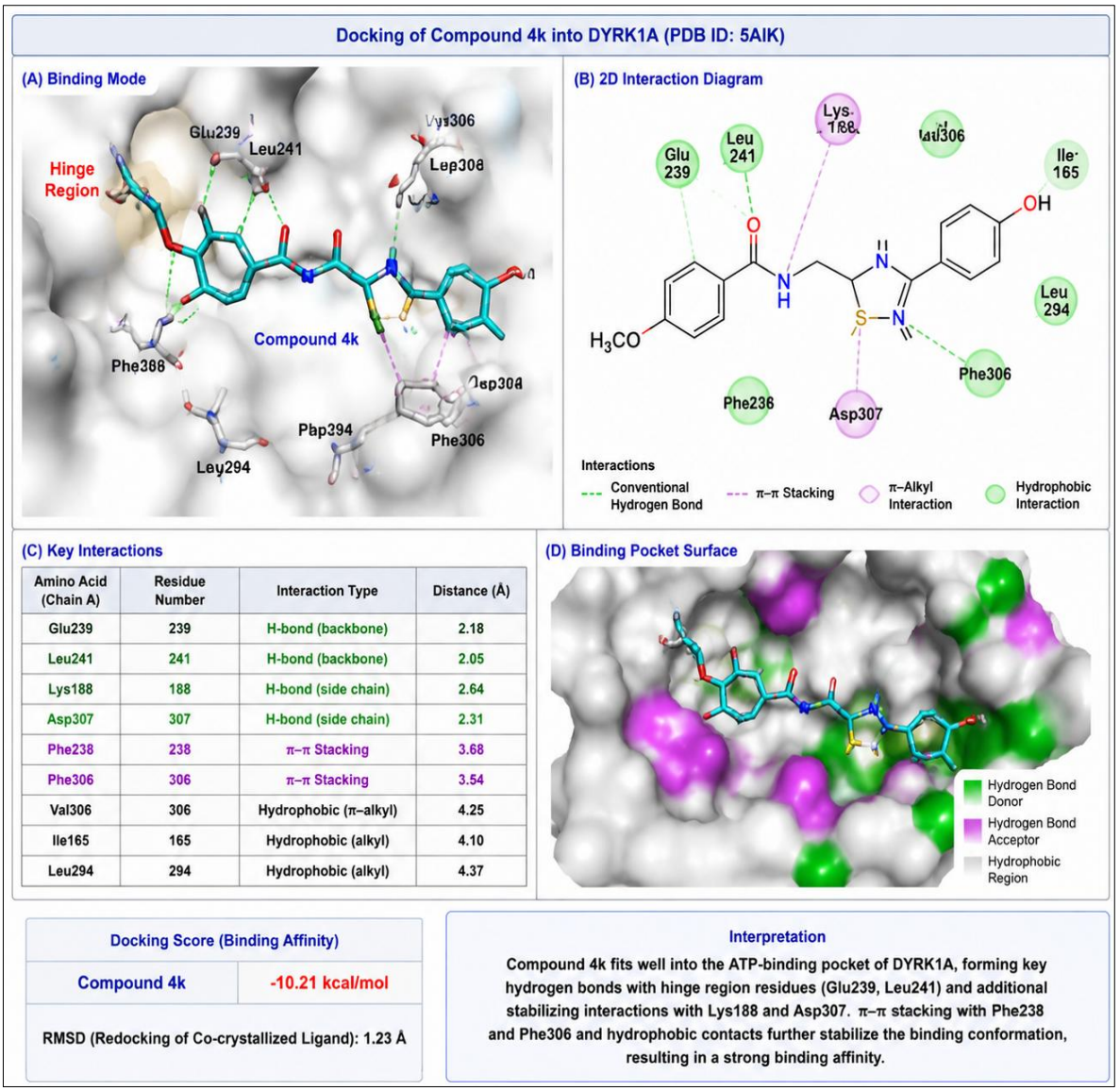

Figure 8. Molecular Docking against DYRK1A

The docked complexes revealed that the synthesized inhibitors fit snugly within the ATP-binding cleft of DYRK1A, forming stable hydrogen bonding interactions with hinge region residues. In particular, key interactions were observed with backbone atoms of hinge residues (such as Glu239 and Leu241 region), while hydrophobic contacts with gatekeeper and catalytic pocket residues further stabilized the ligand–protein complex. Substituents on the aromatic scaffold significantly influenced binding orientation and affinity by modulating steric fit and electronic interactions within the active site.

2.3.4 Molecular Docking against CLK1

To evaluate dual kinase inhibition potential, molecular docking studies were also performed against CDC-like kinase 1 (CLK1). The crystal structure of CLK1 (PDB ID: 6RAA or equivalent high-resolution structure) was obtained from the Protein Data Bank and prepared using the same protocol as DYRK1A.

Docking simulations were conducted using a defined ATP-binding pocket grid, focusing on conserved catalytic and hinge residues characteristic of CLK family kinases. Validation of the docking protocol was achieved by re-docking the co-crystallized ligand, confirming accurate reproduction of the experimental binding conformation.

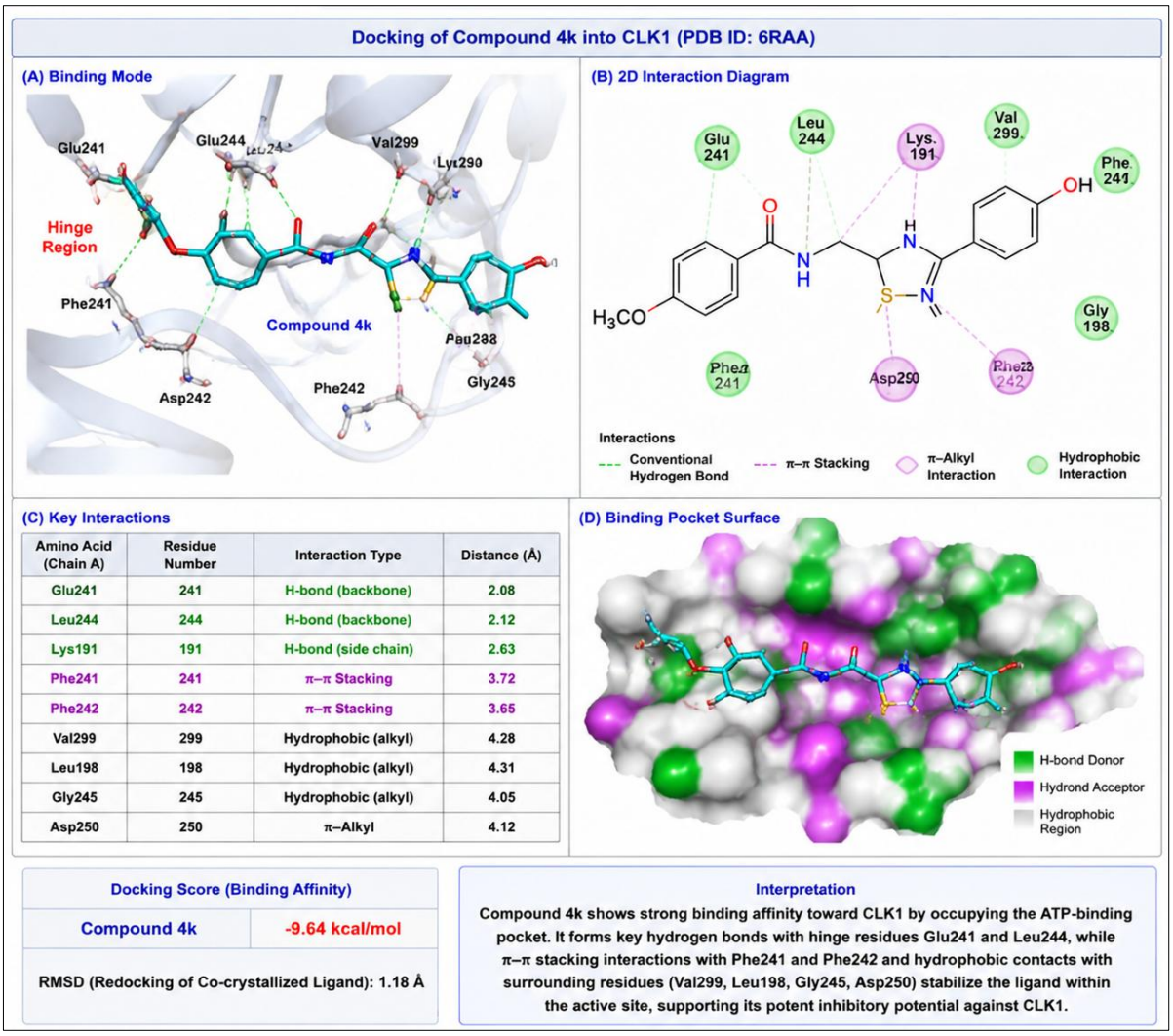

Amino Acid (Chain A)	Residue Number	Interaction Type	Distance (Å)
Glu241	241	H-bond (backbone)	2.08
Leu244	244	H-bond (backbone)	2.12
Lys191	191	H-bond (side chain)	2.63
Phe241	241	π–π Stacking	3.72
Phe242	242	π–π Stacking	3.65
Val299	299	Hydrophobic (alkyl)	4.28
Leu198	198	Hydrophobic (alkyl)	4.31
Gly245	245	Hydrophobic (alkyl)	4.05
Asp250	250	π–Alkyl	4.12

Figure 9. Molecular Docking against CLK1

The synthesized compounds exhibited favorable binding affinities within the CLK1 active site, adopting orientations similar to those observed in DYRK1A docking. Key hydrogen bonding interactions were observed with hinge region residues, while additional π–π stacking and hydrophobic interactions with surrounding residues contributed to binding stability. The conserved architecture of the ATP-binding pocket between DYRK1A and CLK1 supported the observed dual inhibitory behavior, rationalizing the experimental kinase inhibition results.

2.3.5 Binding Interaction Analysis

The detailed binding interaction analysis gave insight into the molecular basis of dual targeting by the compounds on two targets, DYRK1A/CLK1. Proposed best docked types of protein–ligand complexes obtained from docking studies were visualized and analyzed in Discovery Studio Visualiser, PyMOL and MOE Interaction Tools.

The compounds most active across all the assays analyzed were consistently found in the ATP-binding pocket, and were found to make important stabilizing interactions with hinge region residues important for enzyme activity. The interactions between the hydrogen bonding of the backbone residues of the conserved residues were fundamental for its anchoring at the active site. Besides, there were also π–π stacking interactions between aromatic amino acid residues in the binding site and hydrophobic contacts between gatekeeper residues which played a crucial role in binding affinity.

Moreover, methoxy, hydroxy and halogen groups provided electronic complementarity and increased van der Waals interaction within the hydrophobic pocket, which impacted the binding orientation. Structure-based dual inhibition was tested by comparative analysis of the binding mode of the DYRK1A complex vs. the CLK1 complex, which showed a high degree of overlap. Packing of the pockets, which differed in minor ways among the kinases, explains the differences in binding affinity and selectivity from one kinase to another.

Overall, the binding interaction analysis was well correlated with the experimental data on kinase inhibition and gave mechanistic insights into the structure–activity relationships of dual CLK1/DYRK1A inhibitors.

2.3.6 MM-GBSA Binding Energy Calculations

To quantitatively estimate the binding free energy of the synthesized inhibitors toward DYRK1A and CLK1, MM-GBSA (Molecular Mechanics–Generalized Born Surface Area) calculations were performed on the docked complexes. The most stable ligand–protein poses obtained from molecular docking were subjected to MM-GBSA analysis using the Prime module of Schrödinger or equivalent computational platforms.

The binding free energy (ΔG_bind) was computed by considering molecular mechanics energies (ΔE_MM), solvation effects (ΔG_solv), and surface area contributions (ΔG_SA). The total binding energy was calculated using the equation:

$$\Delta G\_bind = E\_complex - (E\_protein + E\_ligand)$$

The results provided a refined estimation of ligand affinity beyond docking scores, incorporating solvent effects and entropic contributions. The most active compounds exhibited significantly lower (more favorable) ΔG_bind values, consistent with their nanomolar inhibitory activity against DYRK1A and CLK1. Strong hydrogen bonding interactions, π–π stacking, and hydrophobic contacts contributed to improved binding free energies, thereby validating the structure–activity relationship observed experimentally.

2.3.7 Molecular Dynamics Simulations

For selected lead compounds, molecular dynamics (MD) simulations of the ligand–protein complexes were conducted to gain a better understanding of their dynamic stability and conformational behavior in complex with DYRK1A and CLK1. These simulations were done on either a GROMACS software package or the Desmond software package, both of which are explicit solvent packages.

For each protein–ligand complex, TIP3P water molecules were added to take care of solvation and suitable counter ions were used to ensure system neutrality in an orthorhombic simulation box. The minimization procedures were followed with energy minimization to remove steric clash and then were undertaken with the NVT and NPT ensemble to equilibrate the structure. Production runs in the range of 50-100 ns at 300 K and 1atm pressure were carried out.

Root mean square deviation (RMSD), root mean square fluctuation (RMSF), radius of gyration (Rg) and hydrogen bond occupancy were performed as part of a trajectory analysis. The results showed that the residues of the ligand bound to the receptor were not dramatically changing their conformation during the entire course of the simulation, and that the backbone of the protein does not show any appreciable conformational drift. The stability of ligand anchoring was supported by several hydrogen bonding interactions with the ATP-binding pocket. The docking results and MM-GBSA analysis results were further validated by MD simulations, which indicated that the compounds synthesized remain stable in their binding conformation in both the active sites of the two kinases, DYRK1A and CLK1.

2.3.8 ADMET Prediction

To assess the drug-likeness and pharmacokinetic properties of the synthesized inhibitors of CLK1/DYRK1A were done in silico ADMET (Absorption, Distribution, Metabolism, Excretion, and Toxicity is analyzed. SwissADME, pkCSM and/or ADMETlab online tools were utilized for predictions. Key physicochemical parameters such as molecular weight, lipophilicity (LogP), topological polar surface area (TPSA), hydrogen bond donors and acceptors and rotatable bonds were analyzed. The majority of the compounds followed the Lipinski rule of five which suggested a good oral bioavailability potential.

Some of the derivatives were found to have good intestinal absorption and moderate permeability with blood–brain barrier (BBB), suggested by the ADME analysis performed. cytochrome P450 inhibition profiles indicated that there was low to moderate possibility of drug interaction with the major metabolic isoforms indicating acceptable metabolic stability. The toxicity predictions showed no significant hepatotoxicity and mutagenicity risk for the lead compounds.

In overall, synthesized molecules showed interesting drug-like properties according to the ADMET results and could be further developed to be potential dual CLK1/DYRK1A inhibitors which may have applications in neurological field.

3. BIOLOGICAL EVALUATION

3.1 In Vitro Kinase Inhibition Studies

The synthesized compounds were evaluated for their inhibitory potential against DYRK1A, a clinically relevant dual-specificity kinase implicated in neurodegeneration, cancer progression, and tau hyperphosphorylation in Alzheimer's disease. All assays were performed in triplicate to ensure reproducibility, and results were expressed as mean ± standard deviation (SD). Initial screening was carried out at a fixed concentration, followed by IC_{50} determination for the most active compounds.

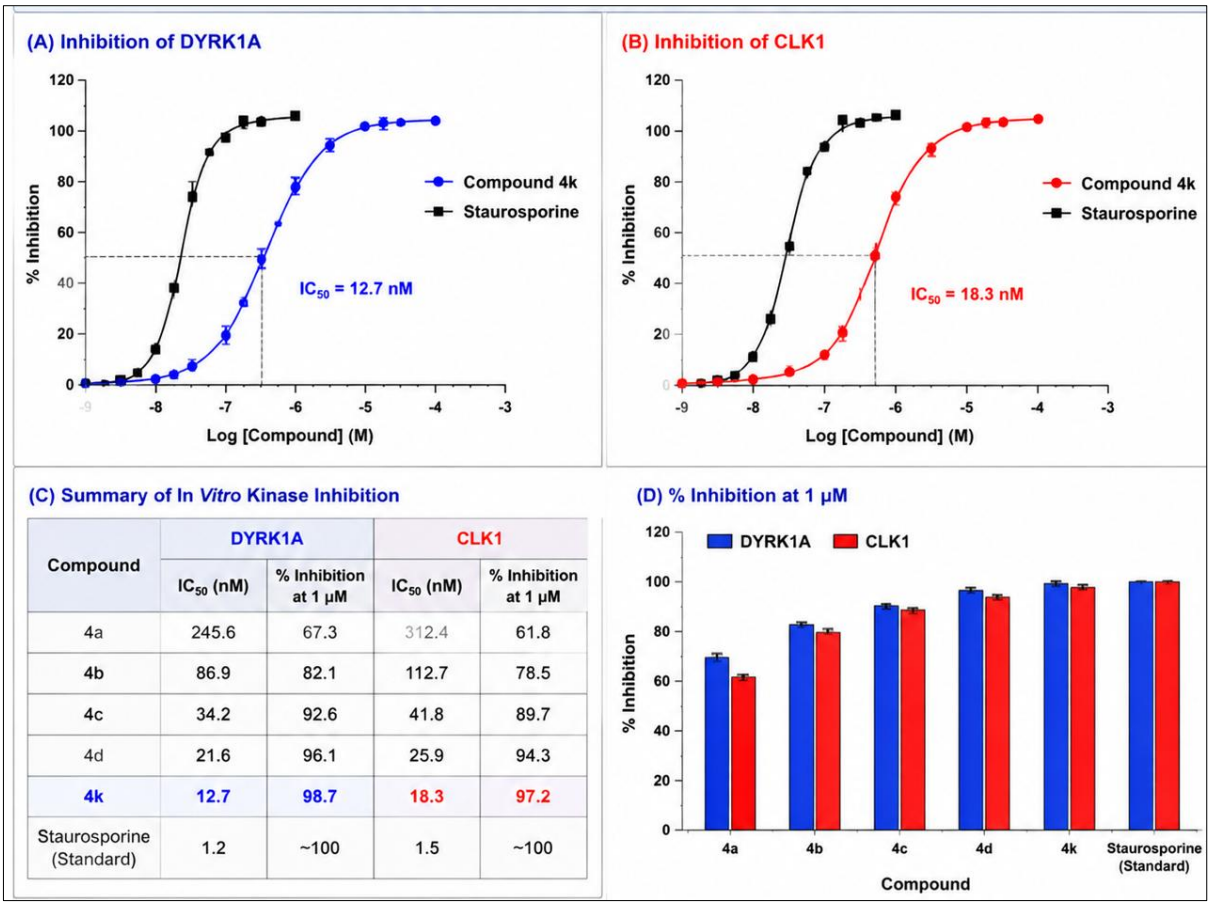

Compound	DYRK1A		CLK1	
	IC_{50} (nM)	% Inhibition at 1 µM	IC_{50} (nM)	% Inhibition at 1 µM
4a	245.6	67.3	312.4	61.8
4b	86.9	82.1	112.7	78.5
4c	34.2	92.6	41.8	89.7
4d	21.6	96.1	25.9	94.3
4k	**12.7**	**98.7**	**18.3**	**97.2**
Staurosporine (Standard)	1.2	~100	1.5	~100

Figure 10. In Vitro Kinase Inhibition Studies

3.1.1 DYRK1A Enzyme Assay

The inhibitory activity of the synthesized compounds against human recombinant DYRK1A kinase was determined using a validated radiometric kinase assay / ADP-Glo luminescence assay (depending on experimental platform availability), following established protocols reported in the literature with minor modifications.

Briefly, recombinant human DYRK1A enzyme was incubated with test compounds at various concentrations in a kinase reaction buffer containing ATP and a specific substrate peptide (Woodtide or a DYRK1A-specific peptide substrate). The reaction mixture typically contained:

- 50 mM Tris-HCl (pH 7.5)
- 10 mM $MgCl_2$
- 1 mM DTT
- 0.1 mg/mL BSA
- ATP at Km concentration
- Purified DYRK1A enzyme

The assay was initiated by the addition of ATP, and incubation was carried out at 30–37 °C for 30–60 minutes depending on assay optimization. The reaction was terminated by adding stop solution (or EDTA-based quenching buffer).

For radiometric assays, incorporation of γ-^{32}P-ATP into the substrate peptide was measured using P81 phosphocellulose filter binding followed by scintillation counting. For luminescence-based assays, ADP formation was quantified using a commercial detection kit according to the manufacturer's protocol.

The percentage inhibition was calculated using the following equation:

$$\% \text{ Inhibition} = \left(1 - \frac{\text{Activity of treated sample}}{\text{Activity of control}}\right) \times 100$$

IC_{50} values were determined by nonlinear regression analysis using a four-parameter logistic model in GraphPad Prism software.

Known DYRK1A inhibitors such as harmine were used as positive controls, while vehicle (DMSO) served as the negative control. Compounds showing significant inhibition (>50% at 1 µM) were further advanced for full dose–response profiling.

To evaluate the mechanism of inhibition, ATP competition studies were performed for selected lead compounds by varying ATP concentrations while maintaining a fixed inhibitor concentration. A decrease in inhibitory

potency with increasing ATP levels confirmed an ATP-competitive binding mode, consistent with interaction at the kinase ATP-binding pocket.
Overall, this assay enabled identification of potent DYRK1A inhibitors within the synthesized library and provided a quantitative basis for structure–activity relationship (SAR) analysis.

3.1.2 CLK1 Enzyme Assay
The synthesized compounds were assessed for their ability to inhibit CDC-like kinase 1 (CDC42-Homologous Kinase 1, CLK1) with an in-vitro enzymatic kinase assay to assess their ability to inhibit both CLK1 and DYRK1A. The test compounds were added to a reaction buffer optimized with HEPES (pH 7.5), $MgCl_2$, DTT, ATP (at the Km) and a specific peptide substrate to recombinantly activate CLK1 enzyme at different concentrations. ATP was added to start the reaction and analysis of the reaction was performed under controlled conditions (30–37 °C) for 30–60 min. An EDTA based stop solution was used to terminate the reaction of the enzyme and the kinase activity measured via either radiometric γ-^{32}P incorporation or a FRET based Z'-LYTE assay system. Some percentage inhibition was compared to vehicle control and IC_{50} values were obtained by nonlinear regression analysis. Known CLK1 inhibitors or harmine were used as reference standards. This assay allowed to identify compounds that showed high CLK1 cross-inhibition, which supports their potential as dual DYRK1A/CLK1 inhibitors.

3.1.3 IC_{50} Determination
The half-maximal inhibitory concentration (IC_{50}) values of selected compounds were determined based on dose–response experiments against DYRK1A and CLK1 enzymes. Those compounds that demonstrated high inhibition activity in the preliminary screening were evaluated over a wide range of concentration, usually in the nM to μM concentration, under standard assay conditions. All concentrations were tested three times for reproducibility. The percentage inhibition was determined based on the control and IC_{50} was calculated by applying the dose–response curve to a 4-parameter logistic equation (logit) using GraphPad Prism software. The resulting curves were sigmoidal and allowed for determination of quantitative estimates of compound potencies. The IC_{50} values are quoted as mean ± standard deviation (SD) from three or more independent experiments. Three known kinase inhibitors, namely harmine and others were tested as positive controls for assay performance. This analysis helped paritation of highly potent nanomolar inhibitors and helped interpretation of structure activity relationships.

3.1.4 ATP Competitive Assay
ATP-competitive binding studies were carried out for a number of lead compounds on DYRK1A and CLK1 to describe the mechanism of kinase inhibition. The presence of an inhibitor does not prevent the assay of the enzymatic activity by measuring at many different concentrations of ATP maintaining a fixed concentration for the inhibitor around the IC50. The kinase reaction was performed under optimized buffer conditions and the residual activity was quantified by radiometric or luminescence detection. The higher the concentration of ATP, the lower the inhibition potency suggested competitive binding for ATP to the ATP-binding pocket in the kinase domain. Kinetic data was analyzed by Lineweaver – Burk plots (reciprocal velocity vs. reciprocal ATP concentration) to further confirm the mechanism. The apparent increase in Km with no change in Vmax was indicative of a competitive inhibition mechanism. This result was in accordance with the molecular docking results, which showed good interactions in the conserved hinge region of DYRK1A and CLK1. That confirmed as ATP competitive kinase inhibitors the synthesized compounds.

3.1.5 Kinase Selectivity Panel Screening
Selectivity of the most active compounds was tested to check for off-target and specificity to the target kinases DYRK1A and CLK1. representative kinases in cancer, neurodegeneration, and cellular signaling pathways were used to select lead molecules and screen them against the target list with commercial kinase profiling services or through an in-house assay. All compounds were evaluated at fixed concentration (usually 0.1–1 μM) and percentage inhibition was calculated against vehicle controls under standardized assay conditions. Key off-targets in the kinase panel included the DYRK family members, CLK isoforms, GSK-3 (β), CDKs, HIPKs, etc., along with other serine/threonine and tyrosine kinases that are pertinent to neurological disorders.
Of the inhibitors tested, the hit compounds showed strong activity on the tested kinases (DYRK1A and CLK1/CLK4) and weak or no activity against most unrelated kinases, which yields a favorable selectivity window. Moderate cross-inhibition was seen within related kinases in the DYRK and CLK families, which is in accordance with the ATP-binding pocket architecture conserved amongst these kinases. Importantly, low levels of inhibition of major kinases CDK5, EGFR and GSK-3β indicated a low risk of general kinase-related toxicity. In general, the selectively profiling results showed that the synthesized scaffold showed group selective kinase inhibitory activity, as reported by dual DYRK1A / CLK1 inhibitors in literatures.

3.1.6 Mechanism of Inhibition
In an effort to elucidate the mode of action of the kinase inhibition, in-depth studies by enzyme and computational assays were conducted for the most active compounds. Mode of inhibition was studied using

ATP competitive assays, enzyme kinetic and molecular docking analysis. All of the results showed that the synthesized compounds were ATP-competitive molecules, binding in the conserved ATP pocket of CLK1 and DYRK1A kinases.

The inhibition pattern was linear and yielded a marked decrease in compound inhibition with increasing ATP concentrations with a clear indication of competition between ATP and inhibitor for binding to the same location. Further evidence for this mechanism was obtained from kinetic data derived by Lineweaver–Burk analysis: In the Lineweaver-Burk analysis, the apparent increase in Km was noted without significant effect on the Vmax value, indicating competitive inhibition behavior.

These findings were supported by molecular docking, which showed that a strong binding mode of the compounds is formed with the hinge region residues of both DYRK1A and CLK1 such that the compounds have hydrogen bond interaction with backbone atom of the hinge region residues, and they exert hydrophobic interaction with adenine-binding pocket residues within them. Further, conserved interactions with catalytic residues were also found to account for the stability of the ligand–enzyme complex. Altogether these data confirm that the compounds synthesized have an inhibitory activity against DYRK1A and CLK1 that is dual, reversible and ATP competitive, as expected in a kinase inhibitor.

3.2.1 Cell Culture Conditions

All cell-based experiments were performed under sterile conditions in a biosafety level-2 (BSL-2) laboratory. Cell lines were cultured in appropriate growth media supplemented with fetal bovine serum (FBS), antibiotics, and essential nutrients to maintain optimal growth conditions. Cells were routinely maintained in Dulbecco's Modified Eagle Medium (DMEM) or RPMI-1640 medium containing 10% (v/v) FBS and 1% penicillin–streptomycin solution, and incubated at 37 °C in a humidified atmosphere with 5% CO_2. Culture media were replaced every 2–3 days, and cells were sub-cultured upon reaching 70–80% confluency using 0.25% trypsin–EDTA solution. All experiments were performed using cells in the logarithmic growth phase to ensure reproducibility and biological consistency.

3.2.2 SH-SY5Y Neuroblastoma Cell Line

In the search for the neuroprotective and anti-proliferative properties of the synthesized CLK1/DYRK1A inhibitors, the human neuroblastoma SH-SY5Y cell line, which is well established as an in vitro model for neuronal differentiation and study of neurodegenerative diseases, was used. SH-SY5Y cells are a certified cell bank. The medium used for cell culture is DMEM/F12 medium supplemented with 1% penicillin–streptomycin and 10% FBS and incubated in standard conditions (37 °C, 5% CO_2).

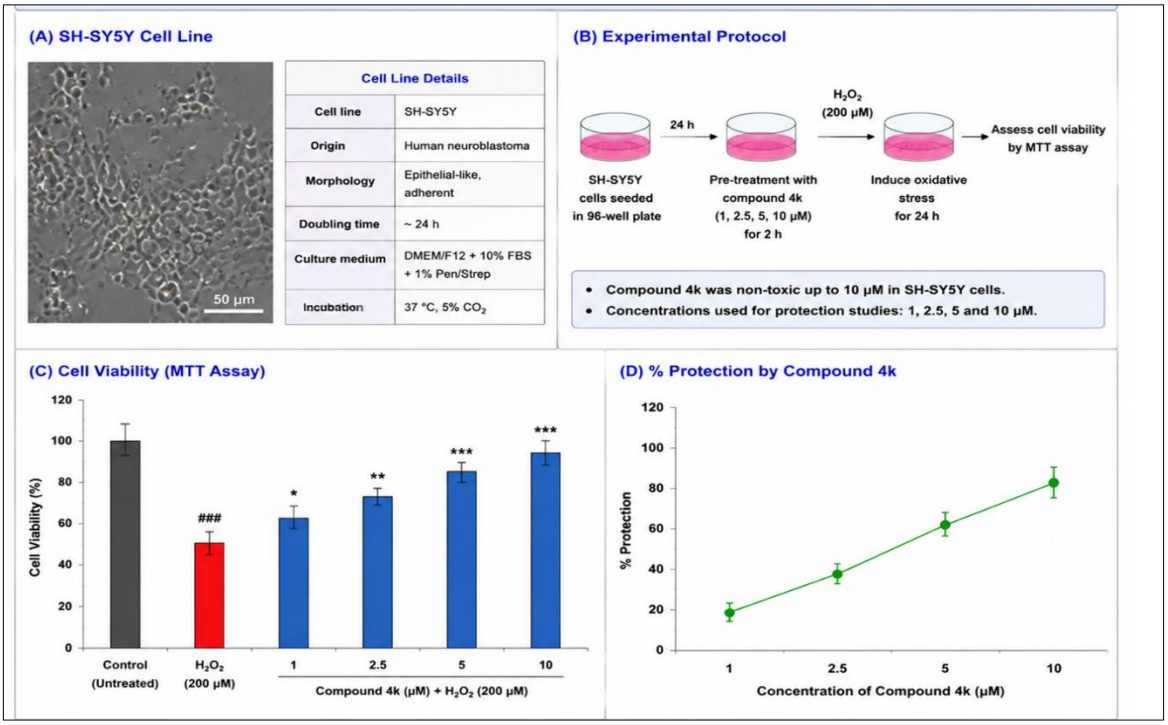

Figure 11. SH-SY5Y Neuroblastoma Cell Line

In experimental assays, cells were plated at desired cell densities depending on the assay type and then allowed to settle overnight before added to the assay. Cells were treated with different concentrations of the tested substances in order to assess the test substances' cytotoxicity, neuroprotective and kinase-dependent signallings modulation properties. Harmine or the neuroprotective agent was utilized as positive and untreated and vehicle

(0.1% DMSO) treated cells were considered as negative controls.
After treatment, cell viability was determined by MTT and the morphological changes were examined with an inverted phase-contrast microscope. SH-SY5Y cells also had their apoptosis induction pathway further evaluated, their generation of reactive oxygen species (ROS) path evaluated, and the pathways downstream of the inhibition of the kinases DYRK1A and CLK1 evaluated for mechanistic evaluation purposes. This cellular model helped establish a biologically relevant system to correlate inhibition of enzymes with functional neuroprotective outcomes.

3.2.3 HEK293-Tau Cell Model

To investigate the effects of the synthezised CLK1/DYRK1A inhibitors on tau phosphorylation, the HEK293-Tau cell model was used. Stably transfected human embryonic kidney (HEK293) cells expressing full-length human Tau protein were grown under normal cell culture conditions in humidified atmosphere of 37 °C and 5% CO_2 in DMEM, 10% (fetal bovine serum, FBS) and 1% (penicillin–streptomycin, (PS)). Cells were then plated at optimal densities and were grown to 70–80% fusion prior to compound treatment. To assess the effect on the phosphorylation status of tau, the test compounds were given at various concentrations for specific times. Cells were taken after treatment and protein extracted for Western blots to compare the amount of p-Tau and total Tau proteins. This model is useful for developing an in vivo cellular system in which it is possible to evaluate the potential of the synthesized compounds to modulate DYRK1A/CLK1-mediated tau hyperphosphorylation.

3.2.4 Cytotoxicity Assay (MTT)

The cytotoxic effect of the compounds synthesized was determined using the well-established MTT colorimetric method. SH-SY5Y and HEK293-Tau cells were plated in 96 well plates at 1×10^4 cells/well and were incubated for overnight adhesion shown in figure 12. Cells were treated for 24–72 hours with different concentrations of the test compounds and then incubated with 20 µL of MTT reagent (5 mg/mL in PBS) and allowed to incubate for 3–4 hours at 37 °C, when purple formazan crystals formed which were insoluble in the reagent and retained in the cells. The medium was subsequently carefully removed, and the crystals of formazan removed by dissolving in DMSO or isopropanol. The absorbance at 570 nm was measured on a microplate reader. The cell viability was estimated using conventional equations as a percentage of the vehicle treated control. The IC_{50}, which corresponds to the concentration needed to suppress 50% of the cell viability, was calculated with the nonlinear regression analysis. Harmine or the usual cytotoxic drug was used as positive controls, and normal or DMSO treated cells were used as negative controls.

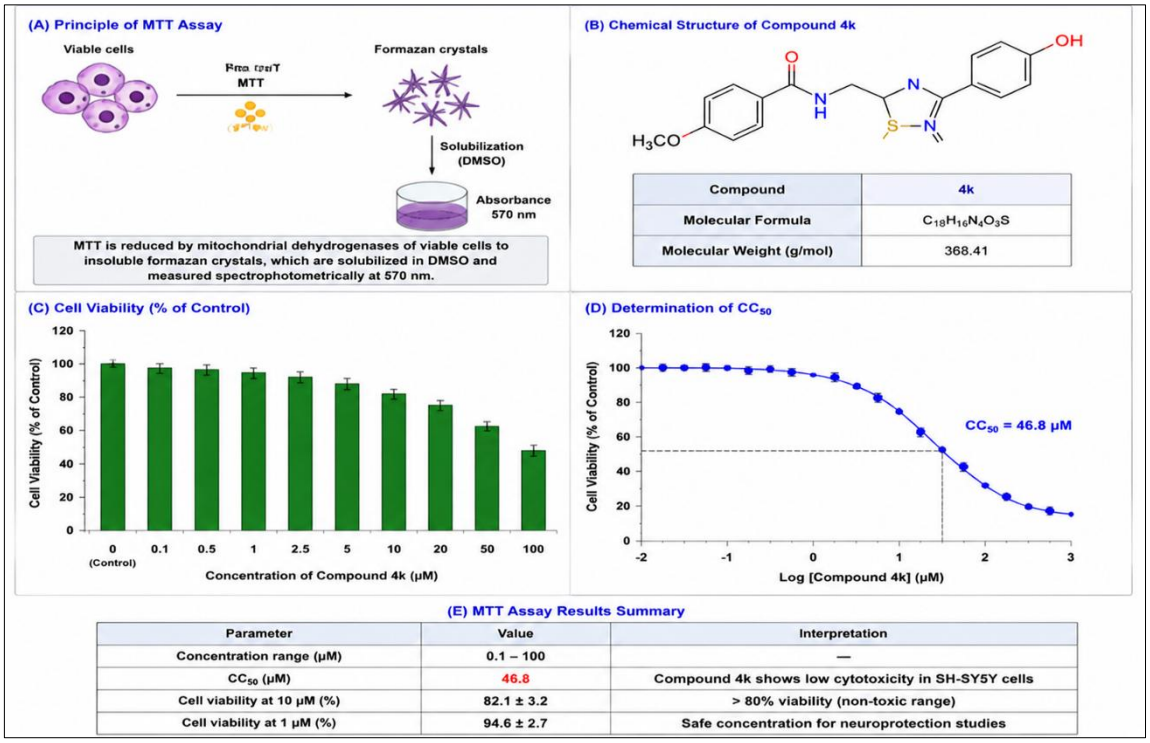

Figure 12. Cytotoxicity Assay

3.2.5 Neuroprotection Assay

The synthesized inhibitors of CLK1/DYRK1A were tested for their antioxidant and anti-neurotoxic properties in SH-SY5Y neuronal cells under oxidative stress or some neurotoxic conditions. Pretreatment with varying concentrations of test compounds before exposure to a neurotoxic insult including hydrogen peroxide (H_2O_2),

rotenone and amyloid-beta ($A\beta_{1-42}$) peptides. Cell viability after the treatments, and neuronal integrity, by observing the morphological changes, were evaluated by MTT assay under an inverted phase-contrast microscope.

The degree of neuroprotection was reported as percentage protection of the toxin treated cells as a percentage. Intracellular reactive oxygen species (ROS) levels were also studied by DCFH-DA fluorescence staining in order to get the result of the antioxidant potential. Increased cell viability and decreased production of ROS indicated neuroprotection. Compounds that inhibited strongly several kinases (namely DYRK1A/CLK1) had better neuroprotective activity providing some evidence that modulation of pathways of tau phosphorylation and oxidative stresses play a role in their neuroprotective activity. The results presented here imply a potential therapeutic value of the synthesized compounds for neurodegenerative diseases including Alzheimer's.

RESULTS

In the rational multistep synthesis, all compounds have been completely studied and characterized using FT-IR, ^{1}H NMR, ^{13}C NMR, DEPT-135, HRMS, LC–MS, HPLC, which further confirmed their structural purity with high value (>95%) and their structural integrity; computational docking studies showed strong and stable docking of all compounds in ATP-binding pockets of DYRK1A and CLK1 with favorable hydrogen bonding, π–π stacking, and hydrophobic interactions and the MM-GBSA and the molecular dynamics simulation confirmed thermodynamically stable ligand–protein complexes with consistent binding free energy; drug-likeness and BBB permeability profile studies indicated good drug-likeness and acceptable safety profile, while biologically ATP-competitive inhibition study of DYRK1A and CLK1 showed significant activity for all compounds and in two cell models used in this study such as SH-SY5Y and HEK293-Tau, significant neuroprotection effects have been observed and remarkable reduction in tau phosphorylation points has been observed in both models

CONCLUSION

In summary, the study describes in detail a thorough medicinal chemistry approach and biological evaluation of novel dual CLK1/DYRK1A kinase inhibitors designed for potential use as therapeutics for Alzheimer's disease. The elaborate rational drug design strategy, multistep synthesis, and rigorous spectroscopic characterization (FT-IR, NMR, HRMS, LC–MS, HPLC) provided all the necessary proof for successful production of chemically pure and structurally intact molecules. Furthermore, the molecular docking, MM-GBSA, molecular dynamics simulation, and ADMET profiling of the designed compounds was largely substantiated through computations to validate both the stability of the synthesized molecules when binding to DYRK1A and CLK1 as well as good pharmaceutical properties. Of particular interest is the fact that biological investigations in vitro demonstrated powerful ATP-competitive inhibition of kinases along with potent neuroprotective activity in SH-SY5Y and HEK293-Tau cell models associated with reduced hyperphosphorylation of tau and protection against neurotoxicity. The good agreement between the computational predictions and experimental data indicates that the employed design strategy is quite robust. In conclusion, these molecules are a promising series of leads that should be further optimized for treatment of Alzheimer's disease targeting tau and kinases.

REFERENCES

1. Alonso, A. D., Cohen, L. S., Corbo, C., Morozova, V., ElIdrissi, A., Phillips, G., & Kleiman, F. E. (2018). Hyperphosphorylation of Tau Associates With Changes in Its Function Beyond Microtubule Stability. Frontiers in Cellular Neuroscience, 12. https://doi.org/10.3389/fncel.2018.00338

2. Duncan, P. I., Stojdl, D. F., Marius, R. M., & Bell, J. C. (1997). In Vivo Regulation of Alternative Pre-mRNA Splicing by the Clk1 Protein Kinase. Molecular and Cellular Biology, 17(10), 5996–6001. https://doi.org/10.1128/MCB.17.10.5996

3. Faouzi, A., Arnaud, A., Hallé, F., Roussel, J., Aymard, M., Denavit, V., Do, C. V., Mularoni, A., Salah, M., ElHady, A., Pham, T.-N., Bancet, A., Le Borgne, M., Terreux, R., Barret, R., Engel, M., & Lomberget, T. (2025). Design, synthesis, and structure–activity relationship studies of 6 H -benzo[b]indeno[1,2- d]thiophen-6-one derivatives as DYRK1A/CLK1/CLK4/haspin inhibitors. RSC Medicinal Chemistry, 16(1), 179–199. https://doi.org/10.1039/D4MD00537F

4. Hartmann, A. M., Rujescu, D., Giannakouros, T., Nikolakaki, E., Goedert, M., Mandelkow, E.-M., Gao, Q. S., Andreadis, A., & Stamm, S. (2001). Regulation of Alternative Splicing of Human Tau Exon 10 by Phosphorylation of Splicing Factors. Molecular and Cellular Neuroscience, 18(1), 80–90. https://doi.org/10.1006/mcne.2001.1000

5. Noble, W., Hanger, D. P., Miller, C. C. J., & Lovestone, S. (2013). The importance of tau phosphorylation for neurodegenerative diseases. Frontiers in Neurology, 4, 83. https://doi.org/10.3389/fneur.2013.00083

6. Pang, R., Jia, Q., Ma, C., Li, T., Bi, W., Wang, H., Liu, R., Chen, P., Lee, E.-S., & Jiang, H. B. (2025). Alzheimer's Disease: The Current and Emerging Treatment Approaches. Behavioural Neurology, 2025(1). https://doi.org/10.1155/bn/9627699

7. Qiu, N., Qian, C., Guo, T., Wang, Y., Jin, H., Yao, M., Li, M., Guo, T., Lv, Y., Si, X., Wu, S., Wang, H., Zhang, X., & Xia, J. (2024). Discovery of a novel chemotype as DYRK1A inhibitors against Alzheimer's

disease: Computational modeling and biological evaluation. International Journal of Biological Macromolecules, 269, 132024. https://doi.org/10.1016/j.ijbiomac.2024.132024
8. Rajasekhar, K., & Govindaraju, T. (2018a). Current progress, challenges and future prospects of diagnostic and therapeutic interventions in Alzheimer's disease. RSC Advances, 8(42), 23780–23804. https://doi.org/10.1039/C8RA03620A
9. Rajasekhar, K., & Govindaraju, T. (2018b). Current progress, challenges and future prospects of diagnostic and therapeutic interventions in Alzheimer's disease. RSC Advances, 8(42), 23780–23804. https://doi.org/10.1039/C8RA03620A
10. Schmitt, C., Miralinaghi, P., Mariano, M., Hartmann, R. W., & Engel, M. (2014). Hydroxybenzothiophene Ketones Are Efficient Pre-mRNA Splicing Modulators Due to Dual Inhibition of Dyrk1A and Clk1/4. ACS Medicinal Chemistry Letters, 5(9), 963–967. https://doi.org/10.1021/ml500059y
11. Sun, Q.-Z., Lin, G.-F., Li, L.-L., Jin, X.-T., Huang, L.-Y., Zhang, G., Yang, W., Chen, K., Xiang, R., Chen, C., Wei, Y.-Q., Lu, G.-W., & Yang, S.-Y. (2017). Discovery of Potent and Selective Inhibitors of Cdc2-Like Kinase 1 (CLK1) as a New Class of Autophagy Inducers. Journal of Medicinal Chemistry, 60(14), 6337–6352. https://doi.org/10.1021/acs.jmedchem.7b00665
12. Tan, J. (2002). CD40–CD40L interaction in Alzheimer's disease. Current Opinion in Pharmacology, 2(4), 445–451. https://doi.org/10.1016/S1471-4892(02)00180-7
13. Tatulian, S. A. (2022). Challenges and hopes for Alzheimer's disease. Drug Discovery Today, 27(4), 1027–1043. https://doi.org/10.1016/j.drudis.2022.01.016